Sensors and Materials, Vol. 36, No. 9 (2024) 3757–3765
MYU Tokyo

S & M 3764

Effect of Annealing Temperature on Photoelectric Properties of ITO:Ga/Ti Thin Films for Photosensor Applications

Wen-Nan Wang, Tsai-Dan Chang, and Tao-Hsing Chen*

Department of Mechanical Engineering, National Kaohsiung University of Science and Technology, Kaohsiung City 807, Taiwan, No. 415, Jiangong Rd., Sanmin Dist., Kaohsiung City 807618, Taiwan

(Received March 20, 2024; accepted June 13, 2024)

Keywords: sputtering, ITO, ITO:Ga, conductive film, vacuum annealing, transparent conducting film

In this study, titanium metal (99.99%) was deposited on quartz glass substrate test specimens by DC magnetron sputtering. Thereafter, radio-frequency magnetron sputtering was used to create an oxide layer of ITO:Ga (97.3 at%) to form a final dual-layer transparent and conductive film on the glass substrate. The film was then annealed at different temperatures under vacuum. The thermal energy rearranged the internal crystalline structure, and this reduced the number of crystalline defects. The multilayer structure of the dual-layer film was explored after annealing: the film thickness, electrical properties, transmission properties, surface structure, grain size, and quality factors were all analyzed. The results showed that the electrical properties of ITO:Ga/Ti improved after annealing at 500 °C (100 W; 30 min) and that the resistivity was 6.51 × 10^{-4} Ω·cm. The average penetration of ITO:Ga/Ti after annealing at 400 °C was 87.52%, and after annealing at 500 °C, it was 89.70%. The figure of merit was the optimal value of 4.78 × 10^{-3} Ω^{-1} after annealing at 500 °C.

1. Introduction

Transparent conducting oxide (TCO) films exhibit excellent conductivity and transmittance characteristics that make them widely applicable in many different optical devices such as solar batteries, film transistors, organic light-emitting parts, and flat liquid-crystal displays.[1–3] The term ‘TCO film’ generally refers to materials consisting of metal oxides. To ensure light transmission in these materials, it is essential to select materials with an energy gap greater than 3 eV. Examples include zinc oxide (ZnO), indium oxide (In_2O_3), titanium dioxide (TiO_2), tin oxide (SnO_2), and cadmium oxide (CdO).[4–7]

To improve the conductivity of metal oxides, special impurities are added to adjust the concentration and type of conductive carrier. This is referred to as doping. The synthesis of TCO films on glass substrates has evolved from spray pyrolysis and chemical vapor deposition (CVD) in the 1940s to vacuum evaporation and sputtering in the 1970s.[8–11] The development of magnetron sputtering in the 1980s facilitated low-temperature film manufacturing and enabled

*Corresponding author: e-mail: thchen@nkust.edu.tw
https://doi.org/10.18494/SAM5049

ISSN 0914-4935
https://myukk.org/

the mass production of films. In recent years, dual-layered structures of an oxide and a metal film that enables higher optical penetration rate and electrical performance have been used. These metal/oxide films can suppress the reflection of the intermediate metal layer in the visible region and achieve higher penetration rate.[12–19]

In this study, DC sputtering was used to deposit Ti as the metal layer and RF sputtering was adopted to deposit ITO:Ga as the oxide layer, forming a film with a dual-layer structure. The resulting test specimens with Ti/ITO:Ga dual-layer films were annealed, after which the thickness, electrical, optical, and structural properties, grain size, and surface pattern were carefully measured to determine the optimal quality parameters of the dual-layer structure. All of the results revealed that the ITO:Ga/Ti thin films were good for solar cell, display, and photosensor applications because of the high photoelectric effect and could be applied in photosensors.

2. Experiment Methods and Materials

In the experiments, the dual layers were deposited by sputtering on 20 × 20 × 2 mm³ quartz glass substrates. These were washed in ethanol in an ultrasonic bath for 10 min, rinsed in deionized water, and dried in an oven at 100 ℃ for 1 h before deposition. Parameters such as sputtering power, sputtering time, and annealing temperature were modified to change the properties of the dual-layer films.[20] The films were annealed by heating the coated specimens under vacuum at 200, 300, 400, and 500 ℃ for 5 min with the temperature increasing 10 ℃ per minute. After this, the effects of annealing temperature on the optical properties and electrical performance of the films were studied. The ITO:Ga oxide layer deposition parameters were set at 100 W with a fixed bias in argon of 6 mTorr, a gas flow rate of 15 sccm, and a sputtering time of 30 min. For the metal layer (Ti), the deposition parameters included a power of 40 W, a fixed bias of 10 mTorr, an Ar gas flow rate of 15 sccm, and a sputtering time of 2.5 min. The dual-layer structure sandwiched the metal layer between the oxide layer and the glass substrate, which prevented the easy oxidation of the metal layer. Furthermore, annealing facilitated the diffusion of the metal layer into the oxide layer, which reduced metal spillage that could lead to poor resistivity. The film thickness was measured using a KLA Alpha-Step stylus profiler Model AS-IQ. The electrical properties were determined using an AHM-800B Hall effect measurement system. The optical properties were measured using a UV-VIS spectrometer (UV Solution 2900). Finally, the surface structure was examined using an atomic force microscope (AFM, Bruker Dimension Fast Scan-XR).

3. Results and Discussion

3.1 XRD structure analysis at different annealing temperatures

Figure 1 shows the results of the XRD analyses of ITO:Ga/Ti films annealed at four different temperatures. It can be seen that the deposited films had an amorphous structure in the as-deposited state, and that, at the annealing temperature of 200 ℃, there were no significant Ti ion

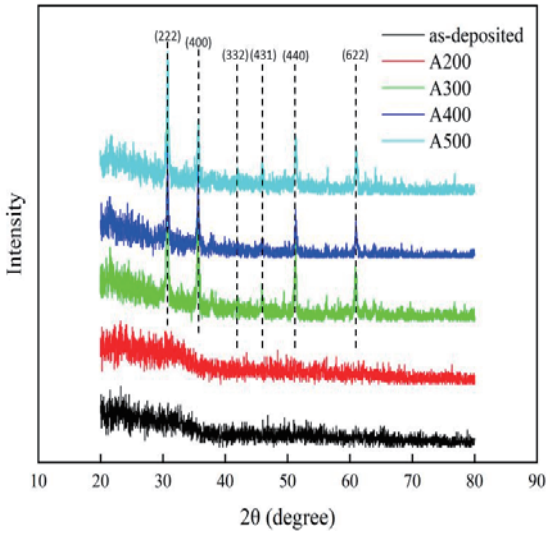

Fig. 1. (Color online) Results of XRD analysis of ITO:Ga/Ti (100 W; 30 min) samples annealed at different temperatures.

peaks and Ti remained evenly distributed over the In_2O_3 lattice. When the annealing temperature was 300 °C, the crystal phase appeared, and as the annealing temperature increased, the peak value of Ti increased. After annealing at 400 °C, the samples contained only the In_2O_3 phase and displayed polycrystalline and cubic bixbyite structures with high-intensity X-ray diffraction. This figure also reveals that Sn atoms might have been substituted into the In_2O_3 lattice.[21] According to Lee *et al.*,[22] the crystallization of ITO occurs at around 150 to 200 °C. In this study, crystallization appeared to be relatively slow and incomplete at 200 °C. At a higher annealing temperature, the intensity of the main diffraction peak (222) on the film surface increased significantly. Annealing at 300 and 400 °C turned the multilayered film into a fully polycrystalline one. The fully annealed ITO layer exhibited the (222) preferential orientation as the annealing treatment of the samples intensified the (222) diffraction peak.[23]

Crystalline phases began to appear in ITO:Ga/Ti films annealed at 300 °C. Peak values of (222), (400), (332), (431), (440), and (622) were found at 30.58, 35.46, 41.85, 45.69, 51.02, and 60.67°, respectively; all of these fall into the peak value range for In_2O_3. This suggested that Ti ions could have been substituted into the In_2O_3 lattice, with (222) as the main direction of growth. The maximum (222) peak occurred in specimens annealed at 500 °C. The thicknesses of each thin film were 93.52 nm for ITO:Ga and 10 nm for Ti.

3.2 Effects of annealing on electrical properties of films

The electrical properties of ITO:Ga/Ti are listed in Table 1; note that good electrical performance could be maintained in samples annealed at 300, 400, and 500 °C. When the thin films were annealed at 200 °C, the grains were still reforming and the resistance presented a slight increase. This implied that the annealing temperature came close to the crystal growth temperature and the crystal arrangement and growth were inhibited, leading to poor electrical

Table 1
Electrical properties of ITO:Ga/Ti in films annealed at different temperatures.

ITO:Ga (100 W; 30 min) / Ti(40 W; 2.5 min)			
Annealing temperature (°C)	Resistivity (Ω·cm)	Mobility (cm^2/Vs)	Carrier concentration (cm^{-3})
As-deposited	2.28×10^{-3}	3.48×10^{1}	7.88×10^{19}
200	7.20×10^{-3}	3.29×10^{1}	2.64×10^{19}
300	1.58×10^{-3}	2.61×10^{1}	1.52×10^{20}
400	8.44×10^{-4}	3.05×10^{1}	2.43×10^{20}
500	6.51×10^{-4}	2.14×10^{1}	4.48×10^{20}

properties. The XRD analysis showed that in the case of thin films that were as-deposited and annealed at 200 °C, the ITO:Ga/Ti film was in an amorphous state. When the thin films were annealed at 300 °C, an In_2O_3 peak appeared and the resistivity increased, caused primarily by a change in carrier concentration. Then, when the annealing temperature was increased to 500 °C, the lowest resistivity of 6.51×10^{-4} Ω·cm was obtained.

3.3 Effects of annealing on optical properties of films

Figure 2 shows the optical properties of the dual-layer film annealed at different temperatures. The overall average transmission for the thin films was approximately 86–89%. Furthermore, the transmission increased slightly with an increase in annealing temperature.

The energy gap was calculated using the optical energy gap formula:[24,25]

$$(\alpha h\upsilon)^2 = A(h\upsilon - Eg), \tag{1}$$

where A denotes a constant and α and $h\upsilon$ represent the absorption coefficient and the incident radiation energy, respectively. Note that a linear relationship exists between $(\alpha h\upsilon)^2$ and $h\upsilon$, which can be used to estimate Eg in Table 2. The as-deposited films had an energy gap of 3.45 eV, and the maximum energy gap at 500 °C was 3.76 eV. The electron energy gap increased with the annealing temperature from 300 to 500 °C. From the average penetration rate, it was observed that the overall change was small and the energy gap did not change considerably. Overall, the energy gap values coincided with those of wide-bandgap semiconductors.

3.4 Analysis of the effects of annealing on film surface features

In this experiment, samples of the sputtered ITO:Ga/Ti dual-layer film on quartz glass substrates were examined by AFM and 3D observations. Average center-line roughness (*Ra*) was measured. Figure 3 shows that the surface of the film became denser and no surface defects such as pores and cracks are visible in the images of samples with high annealing temperatures. Table 3 shows the *Ra* values of the ITO:Ga/Ti thin films. The *Ra* values of the as-deposited thin films and those annealed at 200 °C were less than 1 nm, indicating that the surface of the dual-layer films was very smooth. Moreover, note that the thin films were amorphous before annealing at

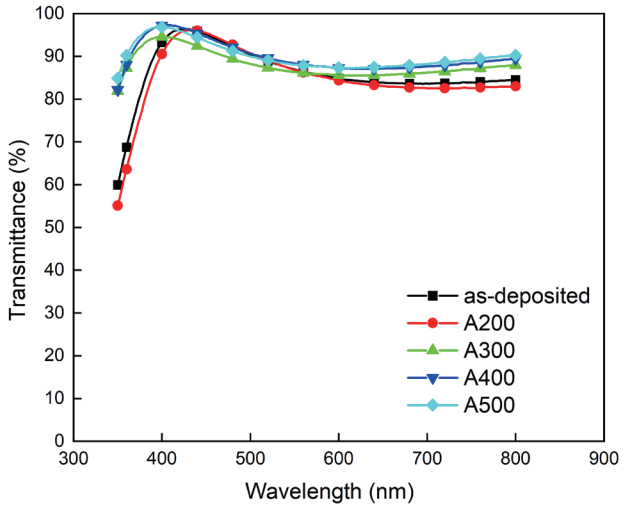

Fig. 2. (Color online) Transmittances of thin films at different annealing temperatures.

Table 2
Energy gap values of ITO:Ga/Ti thin films annealed at different temperatures.

Annealing temperature (°C)	Energy gap (eV)
As-deposited	3.45
200	3.39
300	3.75
400	3.75
500	3.76

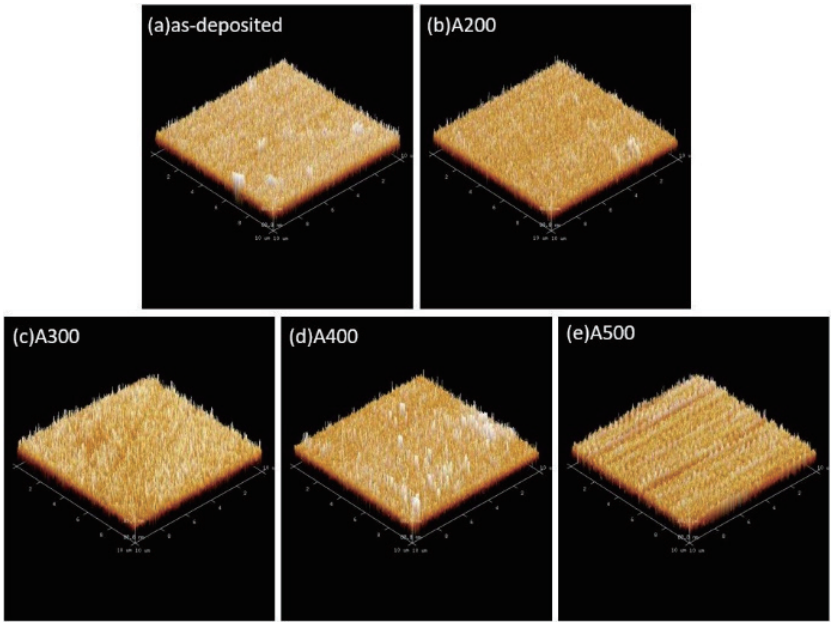

Fig. 3. (Color online) AFM 3D surface features of ITO:Ga/Ti films: (a) as-deposited and annealed at (b) 200, (c) 300, (d) 400, and (e) 500 °C.

Table 3
Ra values of ITO:Ga/Ti films annealed at different temperatures.

Annealing temperature (℃)	*Ra* (nm)
As-deposited	0.99
200	0.91
300	3.42
400	1.13
500	0.50

200 ℃. When the annealing temperature was increased to 300 ℃, the roughness decreased. This could be attributed to the heat-induced rearrangement of the ITO:Ga sample's crystalline structure, which reduced the surface roughness.

3.5 Effect of annealing on crystal grain size

The grain size was calculated by substituting the main XRD peak value into the following Scherrer's formula:[26]

$$D = \frac{0.9\lambda}{\beta \cos\theta}, \tag{2}$$

where D denotes the grain size, λ indicates the incident angle of the X-ray at 0.15418 nm, θ represents the incident angle, and β refers to the full width at half-maximum (FWHM). The FWHM is the width of any intensity distribution at half the maximum intensity of XRD. As λ and θ are constants, there is an inverse relationship between D and β. Therefore, when the FWHM is lower, the grain size is larger. Table 4 shows the FWHM values and grain sizes of ITO:Ga/Ti films annealed at different temperatures. Furthermore, the crystalline phase of ITO:Ga/Ti only appeared in samples annealed at 300 ℃ or above. The FWHM of the films increased with the annealing temperature, and the grain size increased from 32.47 to 37.83 nm. Thus, the increase in annealing temperature led to crystal growth.

3.6 Figure of merit

For transparent conductive films, the figure of merit (FOM) was mainly used for determining the integrity of materials, whereas the resistivity and transmittance were utilized for calculating the FOM (ϕ_{TC}) of dual-layer films at different annealing temperatures using the equation below.

$$\phi_{TC} = \frac{T_{av}^{10}}{R_{sh}} \tag{3}$$

Here, T_{av} denotes the optical average transmittance and R_{sh} indicates the film resistivity in units of Ω^{-1}. This formula shows that the FOM is directly proportional to the 10th power of

Table 4
Effect of annealing temperature on grain size of ITO:Ga/Ti.

ITO:Ga/Ti (100 W; 30 min)		
Annealing temperature (°C)	FWHM	Grain size (nm)
300	0.220	32.47
400	0.233	35.38
500	0.286	37.83

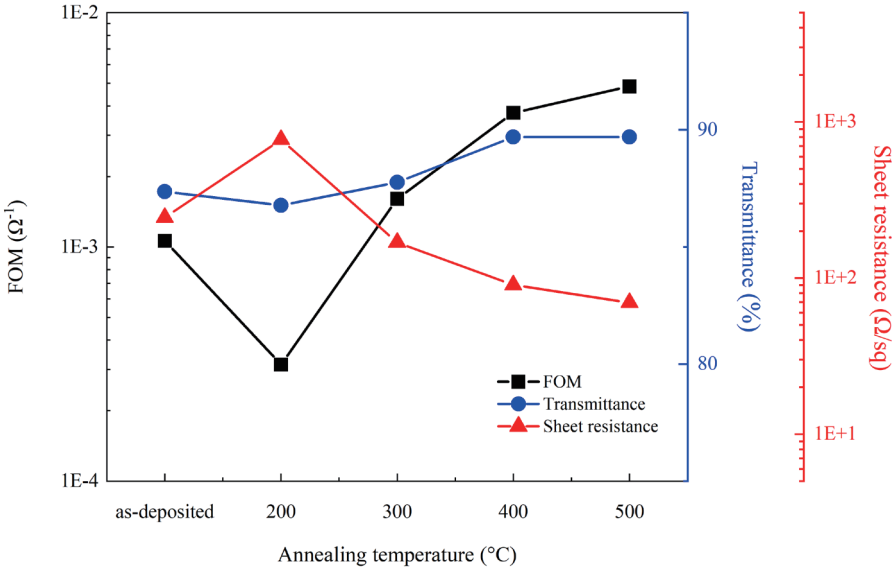

Fig. 4. (Color online) Effect of annealing temperature on FOM of ITO:Ga/Ti thin films.

transmittance. Thus, transmittance had a tremendous effect on FOM. For higher FOM, lower resistivity and higher transmittance rate are necessary.[20,27,28] Figure 4 shows the quality factors of ITO:Ga/Ti films deposited under the conditions of 100 W and 30 min. The optimal FOM was 4.78×10^{-3} Ω^{-1} after annealing at 500 °C. At this annealing temperature, the film had optimal transmittance and low resistivity and hence, excellent FOM.

4. Conclusions

In this study, RF sputtering was used for depositing ITO:Ga/Ti dual-layer films, and the effects of the annealing temperature on the optical and electrical properties of these films were investigated. The results showed that unannealed ITO:Ga/Ti films or those annealed at 200 °C were in an amorphous state. However, upon annealing at 300 °C, a crystalline phase began to emerge and the XRD peak values aligned with those for In_2O_3. This suggested that Ti ions had been substituted into the In_2O_3 lattice with (222) as the primary direction of growth. The crystalline phase reached a peak in samples annealed at 500 °C. The ITO:Ga/Ti film had the lowest resistance of 6.51×10^{-4} Ω·cm after annealing at 500 °C. The optical transmittance of the ITO:Ga/Ti film was the maximum of 89.70% and the energy gap was 3.76 eV after annealing at

500 °C. The AFM analysis of the surface features of the thin films showed that the *Ra* of the ITO:Ga/ Ti thin films was consistently less than 20 nm; in other words, the surface of the dual-layer films was very smooth. Furthermore, as the annealing temperature increased, the roughness *Ra* decreased; this suggested that the annealing process could effectively enhance the smoothness of the film surface. This improvement could be attributed to the rearrangement of ITO:Ga crystals, which caused the surface to become denser. The most significant improvements began after annealing at 300 °C. Finally, the FOM of the ITO:Ga/Ti film had an optimal value of $4.78 \times 10^{-3}\ \Omega^{-1}$ after the film had been annealed at 500 °C. The experimental results proved that the ITO:Ga/Ti thin films could be utilized for making gas sensors, solar cells, and photosensors.

Acknowledgments

This paper was completed as part of Research Project MOST111-2628-E-992-001-MY2, which is supported by the National Science and Technology Council of Taiwan. The authors would like to express their gratitude to the National Science and Technology Council for its support, which enabled the smooth completion of this research. The authors also gratefully acknowledge the use of EM000700 of MOST 110-2731-M-006-001 belonging to the Core Facility Centre of National Cheng Kung University.

References

1 P. Sakthivel, S. Asaithambi, M. Karuppaiah, R. Yuvakkumar, Y. Hayakawa, and G. Ravi: J. Alloys Compd. **820** (2020) 153188. https://doi.org/10.1016/j.jallcom.2019.153188.
2 J. Müller, B. Rech, J. Springer, and M. Vanecek: Solar Energy **77** (2004) 917. https://doi.org/10.1016/j.solener.2004.03.015.
3 S. Singh, V. Sharma, and K. Sachdev: J. Mater. Sci. **52** (2017) 11580. https://doi.org/10.1007/s10853-017-1328-7.
4 B. C. Sertel, N. A. Sonmez, M. D. Kaya, and S. Ozcelik: Ceram. Int. **45** (2019) 2917. https://doi.org/10.1016/j.ceramint.2018.11.079.
5 S. N. Pusawale, P. R. Deshmukh, and C. D. Lokhande: Appl. Surf. Sci. **257** (2011) 9498. https://doi.org/10.1016/j.apsusc.2011.06.043.
6 M. A. Majeed Khan, W. Khan, M. Ahamed, and M. Alhoshan: Mater. Lett. **79** (2012) 119. https://doi.org/10.1016/j.matlet.2012.03.110.
7 K. Badeker: Ann. der Phys. **22** (1907) 749. https://doi.org/10.1002/andp.19073270409
8 H. M. Yates, P. Evans, D. W. Sheel, S. Nicolay, L. Ding, and C. Ballif: Surf. Coat. Technol. **212** (2012) 167. https://doi.org/10.1016/j.surfcoat.2012.10.040.
9 A. Bedia, F. Z. Bedia, M. Aillerie, and N. Maloufi: Superlattices Microstruct. **111** (2017) 714. https://doi.org/10.1016/j.spmi.2017.07.031.
10 W. J. Lee, D. H. Cho, Y. D. Kim, M. W. Choi, J. C. Choi, and Y. D. Chung: J. Alloys. Compd. **806** (2019) 976. https://doi.org/10.1016/j.jallcom.2019.07.321.
11 K. Zhang, F. Zhu, C. H. A Huan, and A. T. S Wee: Thin Solid Films **376** (2000) 255. https://doi.org/10.1016/S0040-6090(00)01418-8.
12 M. Y. Yen, T. H. Chen, P. H. Lai, S. L. Tu, Y. H. Shen, and C.-C. Huang: Sens. Mater. **34** (2022) 175. https://doi.org/10.18494/SAM3555.
13 T. H. Chen and C .L. Yang: Opt. Quantum Electron. **48** (2016) 533. https://doi.org/10.1007/s11082-016-0808-3.
14 M. Y. Yen, T. H. Chen, P. H. Lai, S. L. Tu, and Y. H. Shen: Sens. Mater. **33** (2021) 3941. https://doi.org/10.18494/SAM.2021.3706.
15 T. Y. Tsai, C. J. Liu, T. D. Chang, S. L. Tu, and T. H. Chen: Sens. Mater. **36** (2024) 671. https://doi.org/10.18494/SAM4684.
16 S. M. Rozati and S. A. M. Ziabari: Mater. Chem. Phys. **292** (2022) 126789. https://doi.org/10.1016/j.matchemphys.2022.126789.

17 S. Y. Lee: Opt. Mater. **112** (2021) 110820. https://doi.org/10.1016/j.optmat.2021.110820.
18 T. H. Chen, T. C. Cheng, and Z. R. Hu: Microsyst. Technol. **19** (2013) 1787. https://doi.org/10.1007/s00542-013-1837-5.
19 H. Kong and H. Y. Lee: Thin Solid Films **696** (2020) 137759. https://doi.org/10.1016/j.tsf.2019.137759.
20 G. Haacke: J. Appl. Phys. **47** (1976) 4086. https://doi.org/10.1063/1.323240.
21 M. Gulen, G. Yildirim, S. Bal, A. Varilci, I. Belenli, and M. Oz: J. Mater. Sci.-Mater. Electron. **24** (2013) 467. https://doi.org/10.1007/s10854-012-0768-8.
22 K. S. Lee, Y. J. Mo, I. K. Park, T. S. Park, and Y. S. Kim, Bull. Korean Chem. Soc. **41** (2020) 341. https://doi.org/10.1002/bkcs.12000.
23 P. Prepelita, M. Filipescu, I. Stavarache, F. Garoi, and D. Craciun: Appl, Surf, Sci. **424** (2017) 368. https://doi.org/10.1016/j.apsusc.2017.02.106.
24 T. Minami, H. Nanto, and S. Takata: J. Appl. Phys. **24** (1985) L605. https://doi.org/10.1143/JJAP.24.L605.
25 Y. C. Chang, T. H. Chen, T. D. Chang, S. L. Tu, and Y. H. Shen: Sens. Mater. **35** (2023) 2871. https://doi.org/10.18494/SAM4354.
26 M. Caglar, S. Ilican, and Y. Caglar: Thin Solid Films **517** (2009) 5023. https://doi.org/10.1016/j.tsf.2009.03.037.
27 C. F. Liu, T. H. Chen, and Y. S. Huang: Sens. Mater. **32** (2021) 2321. https://doi.org/10.18494/SAM.2020.2867.
28 C. F. Liu, S. C. Shi, T. H. Chen, and G. L. Guo: Sens. Mater. **34** (2022) 4127. https://doi.org/10.18494/SAM4133.

About the Authors

Wen-Nan Wang received his M.S. degree from Chi-Yi University, Taiwan, in 2022. Currently, he is a Ph.D. student at the Department of Mechanical Engineering, National Kaohsiung University of Science and Technology. Since 2010, he has been the general manager of Shieh Ho Tien Enterprise Co., Ltd. His research interests include optical materials, heat transfer, fluid sensors, and pressure sensors.

Tsai-Dan Chang received her B.S. degree from National Kaohsiung University of Science and Technology, Taiwan, where she is currently studying for her M.S. degree. Her research interests include TCO thin films, materials engineering, and sensors.

Tao-Hsing Chen received his B.S. degree from National Cheng Kung University, Taiwan, in 1999, and his M.S. and Ph.D. degrees from the Department of Mechanical Engineering, National Cheng Kung University, in 2001 and 2008, respectively. From August 2008 to July 2010, he was a postdoctoral researcher at the Centre for Micro/Nano Science and Technology, National Cheng Kung University. In August 2010, he became an assistant professor at National Kaohsiung University of Applied Sciences (renamed National Kaohsiung University of Science and Technology), Taiwan. Since 2016, he has been a professor at National Kaohsiung University of Science and Technology. His research interests include metal materials, TCO thin films, thermal sensors, and photosensors. (thchen@nkust.edu.tw)